J|A|C|S
ARTICLES
Published on Web 10/02/2004

In Situ Disorder−Order Transformation in Synthetic Gallosilicate Zeolites with the NAT Topology

Suk Bong Hong,*,† Song-Ho Lee,† Chae-Ho Shin,‡ Ae Ja Woo,§ Luis J. Alvarez,|| Claudio M. Zicovich-Wilson,⊥ and Miguel A. Camblor#

Contribution from the Division of Chemical Engineering, Hanbat National University, Taejon 305-719, Korea, Department of Chemical Engineering, Chungbuk National University, Chungbuk 361-763, Korea, Department of Science Education, Ewha Womans University, Seoul 120-750, Korea, Instituto de Matématicas (U. Cuernavaca), Universidad Nacional Autónoma de Mexico, 62210 Cuernavaca (Mor), Mexico, Facultad de Ciencias, Universidad Autónoma del Estado de Morelos, 62210 Cuernavaca (Mor), Mexico, and Instituto de Ciencia de Materiales de Madrid, Consejo Superior de Investigaciones Científicas, Campus Cantoblanco, 28049 Madrid, Spain

Received May 25, 2004; E-mail: sbhong@hanbat.ac.kr

Abstract: Here, we report that synthetic gallosilicate molecular sieves with the NAT topology and Si/Ga ratios close to but slightly higher than 1.50 undergo an in situ transformation under their crystallization conditions. The materials have been studied ex situ by using powder X-ray diffraction, elemental and thermal analyses, and multinuclear MAS NMR. The transformation is characterized by a change in the distribution of Si and Ga of the NAT framework, from a quite (but not completely) disordered phase to a very highly (but not completely) ordered one, accompanied by a change from tetragonal to orthorhombic symmetry. During most of the solution-mediated transformation, no noticeable signs of fresh precipitation, phase segregation, or changes in the chemical composition are detected. Intermediate materials show variations in the degree of Si−Ga ordering and orthorhombic distortion and are not physical mixtures of the disordered and ordered phases. Ab initio calculations strongly suggest a preferential siting of Si in the tetrahedral sites involved in a smaller number of 4-rings in the NAT topology (i.e., the low multiplicity site). The cost of violations of Loewenstein's rule has also been calculated. For this topology and chemical composition the preferential siting and Loewenstein's rule drive together the system to the ordered configuration. A Monte Carlo sampling procedure affords a reasonable model for the initial, mainly disordered state, which fits well within the experimental disorder−order series.

1. Introduction

Zeolites are a class of microporous solids that are built by full corner sharing of TO_4 tetrahedra through single T−O−T bridges, yielding a three-dimensional four-connected network, where T is Si or Al. While this classical definition can be relaxed to include a number of additional elements, e.g., P, Ga, B, Be, Zn, etc., with various formal oxidation states, the tetrahedron has one negative charge or more for T-atoms with oxidation states below 4. However, there is avoidance for the pairing of charged tetrahedra in hydrothermally synthesized zeolites according to the so-called Loewenstein's rule.[1] When more than one type of T-atom is present, in particular, the question of their distribution among the available tetrahedral sites (T-sites), together with the observance of Loewenstein's rule, arises.

To date, there is a growing list of zeolites where the spatial distribution of heteroatoms other than Si proved to be nonrandom,[2−8] reflecting the preference of a given heteroatom for certain kinds of crystallographically distinct T-sites. Elucidating the precise reasons for this phenomenon may be of considerable interest for systematically controlling many important properties of zeolites at the molecular level, most notably their Brønsted acidity, and hence for finding more successful applications as commercial catalysts and separation media in the petrochemical and refining industries. The site-specific introduction of heteroatoms into zeolite frameworks also has important implications in "structure direction", i.e., in driving the crystallization toward microporous materials with specific topologies. This strategy has been successfully used as an additional tool for the discovery of new topologies and, in some

† Hanbat National University.
‡ Chungbuk National University.
§ Ewha Womans University.
|| Universidad Nacional Autónoma de Mexico.
⊥ Universidad Autónoma del Estado de Morelos.
Instituto de Ciencia de Materiales de Madrid.

(1) Loewenstein, W. *Am. Mineral.* **1954**, *39*, 92.
(2) Han, O. H.; Kim, C.-S.; Hong, S. B. *Angew. Chem., Int. Ed.* **2002**, *41*, 469.
(3) Kennedy, G. J.; Afeworki, M.; Hong, S. B. *Microporous Mesoporous Mater.* **2002**, *52*, 55.
(4) Abraham, A.; Lee, S.-H.; Shin, C.-H.; Hong, S. B.; Prins, R.; van Bokhoven, J. A. *Phys. Chem. Chem. Phys.* **2004**, *6*, 3031.
(5) Cheetham, A. K.; Fjellvag, H.; Gier, T. E.; Kongshaug, K. O.; Lillerud, K. P.; Stucky, G. D. *Stud. Surf. Sci. Catal.* **2001**, *135*, 158.
(6) Annen, M. J.; Davis, M. E.; Higgins, J. B.; Schlenker, J. L. *J. Chem. Soc., Chem. Commun.* **1991**, 1175.
(7) Rohrig, C.; Gies, H. *Angew. Chem., Int. Ed.* **1995**, *34*, 63.
(8) Park, S. H.; Daniels, P.; Gies, H. *Microporous Mesoporous Mater.* **2000**, *37*, 129.

10.1021/ja046921h CCC: $27.50

instances, for the a priori design of zeolites with predetermined structural features. For instance, Be and Zn have been shown to give rise frequently to structures with the rather unusual spiro-5 unit, where these heteroatoms occupy corners of that unit.[5−7] Very recently, Li has also shown such an ability to promote the formation of new zeolitic structures with the same building unit, although Li accommodates itself at the center of the spiro-5 unit.[8] All these cases appear to be related to a preferential siting of Be, Zn, and Li, i.e., to their preference to occupy certain types of T-sites with relatively small T−O−T angles.

In the course of our current synthetic program at the Hanbat National University to investigate the structure-directing effects of Ga,[9−12] we have synthesized two different versions of a gallosilicate zeolite with the same topology (NAT), the same chemical composition (Si/Ga ≈ 1.5) but with different T-atom distributions. These two gallosilicate materials were found to be the disordered tetragonal ($I\bar{4}2d$) and ordered orthorhombic (*Fdd*2) end members, respectively,[10,12] of the NAT family of zeolites containing a three-dimensional pore system with 8- and 9-ring channels.[13] We have also shown that their crystallization, thought at that time to be independent of each other, can be controlled by just varying the crystallization temperature, while both materials crystallize from the same starting mixture compositions. This phenomenon appeared as puzzling, since the difference between the two phases is related to the splitting of a crystallographic site that is topologically unique and, apparently, ordering of Si and Ga atoms is not governed only by the "extended" Loewenstein's rule (i.e., avoidance of Ga−O−Ga bonds) for this topology and Si/Ga ratio. Here we will show that the crystallization of these phases is not independent: at a given temperature the initial disordered crystalline material slowly transforms in situ into the ordered version and hence materials with any intermediate degree of order can also be synthesized. We will also show that these intermediate materials are not physical mixtures of the disordered and ordered versions; i.e., there is no phase segregation during the transformation. The details of the disordered and ordered states, their transformation, and its driving force, as well as the reason for such ordering, are the issues to be addressed, with the help of both experimental and theoretical approaches. This study provides an example on how Loewenstein's rule, framework topology, preferential siting, and Si/Ga ratio may impose onto the T-atom distribution.

2. Experimental Section

2.1. Zeolite Synthesis. The following procedure was used for the synthesis of microporous gallosilicate materials with NAT topology. In a typical synthesis, 7.11 g of NaOH (50% aqueous solution, Aldrich) and 1.39 g of gallium oxide (Ga_2O_3, 99.99+%, Aldrich), and 8.98 g of deionized water were mixed in a plastic vessel and heated overnight at 100 °C. To the resulting clear solution, after cooling to room temperature, 11.11 g of colloidal silica (Ludox AS-40, DuPont) was added. The oxide composition of the final synthesis mixture can be expressed as $6.0Na_2O{\cdot}1.0Ga_2O_3{\cdot}10.0SiO_2{\cdot}150H_2O$. The synthesis mixture was stirred at room temperature for 1 day, charged into Teflon-lined 45-mL autoclaves, and heated at 150 °C, with or without stirring (60 rpm) under autogenous pressure, for 1−23 days. The synthesis of NAT-type gallosilicates was also performed at 100 °C for 1−7 days and at 200 °C for 14−28 days. The solid products were recovered by filtration, washed repeatedly with water, and then dried overnight at room temperature. If required, as-made materials in the Na form were refluxed twice in 1.0 M KNO_3 solutions overnight in order to convert them into their K form.

TNU-3 and TNU-4 notations have been previously used to denote the almost disordered and ordered gallosilicates with the NAT topology, respectively.[10,12] Although we always use the same starting composition in the present study, the degree of ordering of Si and Ga atoms in all materials prepared here depends on the synthesis temperature and time (see below). Thus, for convenience, the materials in this work will be denoted as a function of the synthesis conditions as NAT-T-t, where T and t stand for the synthesis temperature in centigrades and time in days, respectively. Also, materials prepared under static conditions will be referred as NAT-T-t-s.

2.2. Characterization. Powder X-ray diffraction (XRD) data were collected on a Rigaku 2500H diffractometer with Cu Kα radiation (40 kV and 200 mA). The samples were analyzed in the 2θ range 10°−45° with a step size of 0.01° and a count time of 1 s per step. Unit cell parameters were obtained by full-profile fitting of the powder XRD data using the program EXPO.[14] In situ high-temperature XRD experiments were carried out on a Scintag XDS 2000 diffractometer equipped with an Edmund Bühler HDK 1.4 high-temperature attachment. Elemental analysis was performed by a Jarrell-Ash Polyscan 61E inductively coupled plasma (ICP) spectrometer in combination with a Perkin-Elmer 5000 atomic absorption spectrophotometer. Thermogravimetric and differential thermal analyses (TGA/DTA) were carried out in air on a TA Instruments SDT 2960 thermal analyzer at a heating rate of 10 °C min^{-1}.

The ^{29}Si MAS NMR spectra were measured on a Bruker DSX 400 spectrometer operating at a spinning rate of 12.0 kHz at a ^{29}Si frequency of 79.490 MHz with a $\pi/5$ rad pulse length of 2.0 μs. Long recycle delays of 40−60 s were used to avoid relaxation effects in the signal intensities. Typically, 1000−1200 pulse transients were accumulated, and the ^{29}Si chemical shifts are referenced to TMS. Spectral deconvolution and simulation were performed using mixed Gaussian−Lorentzian curves with the Origin curve-fitting software. The ^{71}Ga MAS NMR spectra were recorded at room temperature and 150 °C on the same spectrometer operating at a ^{71}Ga frequency of 122.040 MHz and a spinning rate of 10.0 kHz. The spectra were obtained with an acquisition of ca. 2000 pulse transients, which was repeated with a $\pi/4$ rad pulse length of 1.0 μs and a recycle delay of 0.1 s. The ^{71}Ga chemical shifts are reported relative to a $Ga(H_2O)_6^{3+}$ solution. The ^{23}Na MAS NMR spectra at room temperature and 150 °C were obtained at a ^{23}Na frequency of 105.863 MHz and a spinning rate of 10.0 kHz. The spectra were obtained with an acquisition of ca. 600 pulse transients, which were repeated with a pulse length of 1.0 ms and a recycle delay of 3 s. The ^{23}Na chemical shifts are reported relative to a NaCl solution.

2.3. Numerical Simulation Details. To describe the materials that have been crystallized under different hydrothermal synthesis conditions and that have different degrees of order in the distribution of Si and Ga atoms, we have first used a Monte Carlo sampling procedure. Since all these materials have the same topology and only differ in the cation distribution, the model employed for the NAT framework in the Monte Carlo sampling considers only the T-site sublattice. Therefore, only the T−T connectivity table and the occupancy of each site are necessary

(9) Hong, S. B.; Kim, S. H.; Kim, Y. G.; Kim, Y. C.; Barrett, P. A.; Camblor, M. A. *J. Mater. Chem.* **1999**, *9*, 2287.
(10) Cho, H. H.; Kim, S. H.; Kim, Y. G.; Kim, Y. C.; Koller, H.; Camblor, M. A.; Hong, S. B. *Chem. Mater.* **2000**, *12*, 2292.
(11) Kim, S. H.; Kim, S. D.; Kim, Y. C.; Kim, C.-S.; Hong, S. B. *Microporous Mesoporous Mater.* **2001**, *42*, 121.
(12) Paik, W. C.; Camblor, M. A.; Hong, S. B. *Stud. Surf. Sci. Catal.* **2001**, *135*, 244.
(13) International Zeolite Association, Structure Committee, http://www.iza-structure.org.
(14) Altomare, A.; Burla, M. C.; Camalli, M.; Carrozzini, B.; Cascarano, G.; Giacovazzo, C.; Guagliardi, A.; Moliterini, A. G. G.; Polidori, G.; Rizzi, R. *J. Appl. Crystallogr.* **1998**, *32*, 339.

to characterize the different distributions. There are two different nonequivalent T-sites under the topological symmetry group, namely T_1 and T_2, of multiplicity 16 and 4, respectively. The former are all components of the "equatorial" 4-rings of the NAT building unit and are connected to three other T_1 and one T_2 sites, while the latter are bridges between opposite corners of those rings and are only connected to T_1 sites.

The Monte Carlo configuration sampling procedure is as follows. A proposed configuration is generated by randomly choosing one Si atom and one Ga atom to exchange their positions in the connectivity table. If the extended Loewenstein's rule is violated by this exchange, the proposed configuration is accepted with a relatively low probability. If there is no violation of Loewenstein's rule, then the proposed configuration is accepted. The formal expression of this acceptance/rejection rule is derived from the two-color Potts' function given by Wu:[15]

$$p(T^{(M)}|M) = \frac{1}{Z_\beta}\exp\{\sum_{\{i,j\}}\beta_{ij}[T(i), T(j)]\} \qquad (1)$$

where the sum is over all pairs $\{i,j\}$ of T−T neighbors, $T(i)$ gives the atom type (Ga or Si) occupying position i in the framework, Z_β is a normalizing constant, and

$$\beta_{ij}\,[T(i),T(j)] = \begin{Bmatrix} -1 & \text{if } T(i)=T(j)=\text{Ga} \\ 1 & \text{otherwise} \end{Bmatrix}$$

This function gives the prior probability of a given configuration with M T-sites per unit cell. Additional constraints are to be considered due to the fact that there are preferential sites for cation location. Therefore, eq 1 has to be transformed into

$$p(T^{(M)}|M) = \frac{1}{Z_\beta}\exp\{\sum_{\{i,j\}}\beta_{ij}[T(i), T(j)] + \sum_i \gamma_i[T(i)]\} \qquad (2)$$

where the second sum in the argument of the exponential function is over the M T-sites and $\gamma_i[T(i)]$ can have four different values corresponding to combinations between the two types of cations, $T(i)$ = Si, Ga, and the two types of sites, $i = T_1, T_2$. The $\gamma_i[T(i)]$ values will depend on the relative stabilities of the local cation arrangements in the framework, and in this work they have been estimated by means of periodic ab initio calculations (vide infra). The acceptance rule of the Monte Carlo procedure is given by the condition that the ratio $p/p' < 1$, where p and p' are the probabilities of the current and proposed configurations, respectively. With this criterion, a large number of configurations are generated starting from the perfectly ordered orthorhombic structure. In practice, this strategy is similar to that used in a previous work,[16] although each one is based on different formal frameworks.

To obtain a suitable acceptance rule for the sampling procedure, it is sufficient to state the relative weights of the contributions of the second sum with respect to the first one, in the exponential of the Potts' function. From the physical point of view one expects these weights to be proportional to the energy cost of each kind of exchange event involved. Accordingly, the first sum changes by +2 each time a given Si−Ga exchange introduces one violation of Loewenstein's rule. Considering the ab initio exchange energies (vide infra), the energetic cost of a Loewensteinian violation is about 4 times, in absolute value, the gain provided by the exchange of a Ga in T_1 with a Si in T_2. Satisfying this ratio, a suitable parametrization for the Monte Carlo sampling is that $\gamma_i[T(i)] = -1/2$ when site i is T_2 and $T(i)$ = Ga and 0 otherwise. The factor Z_β in eq 2 has been chosen so as to keep a reasonable equilibrium between degree of penalization and computational cost. In this work, a Z_β value of −50 yielded a low percentage of violations of Loewenstein's rule (<0.3%) and a reasonable computational performance.

Table 1. Structural Specifications and Calculated Total ab Initio Energies per Primitive Cell of the NAT Models[a]

model	crystal system	Si/Ga	no. of point symmetry operators	Ga site	energy, Hartree
ω_1	orthorhombic	1.5	4	T'_1	−11 590.4827
τ_1	tetragonal	1.5	4	T_1	−11 590.4342
τ_2	tetragonal	4.0	2	T_1	−7995.3998
τ_3	tetragonal	4.0	2	T_2	−7995.3940

[a] Optimized geometries given in Supporting Information Table 1S.

In the course of the sampling process there are three well-defined stages. In the first one, configurations are slight variations of the orthorhombic structure. After a small number of steps there is a transition stage in which Loewenstein's rule is violated in relatively low proportions. In the third stage the system falls in a semi-disordered state with practically no violations of Loewenstein's rule. This third stage is the one in which we are interested. The criterion to decide whether the system is at this stage is that the fluctuation of the Potts' function to be less than a given threshold (10^{-7}). At this stage the sampling process is initiated taking one out of 100 configurations to calculate statistics. Sampling went on for 5×10^6 accepted configurations. The Monte Carlo sampling has been performed considering a periodic framework in which the unit cell is an expansion of the NAT conventional cell. The supercell has new cell parameters given by: $a' = 5a$, $b' = 5b$, $c' = 10c$. Using this expansion the cell shape is close to cubic the border constraints being minimized. The number of T-sites in the system is 5000, and Si/Ga ratios equal to 1.50, 1.53, 1.55, and 1.58 have been considered for sampling.

Periodic ab initio calculations have also been performed employing the LCAO approximation as implemented in the CRYSTAL98 code.[17] The B3LYP Hamiltonian[18,19] has been employed with a basis set of split-valence double-ζ quality with additional polarization functions in oxygen atoms.[20] All structures have been fully optimized under symmetry constraints and keeping the lattice parameters constant to $a = b = 13.197$ Å, $c = 6.663$ Å, $\alpha = \beta = \gamma = 90°$, which are those exhibited by our sample NAT-100-3-s. Optimizations have been performed using gradient techniques, as recently implemented in the CRYSTAL code.[21,22] Several structures have been considered for calculation in order to determine their relative stabilities. The most relevant structural characteristics are summarized in Table 1, and their atomic coordinates can be found in Supporting Information Figure 1S. In all cases, the chemical composition per primitive cell is $Na_xGa_xSi_{10-x}O_{20}$. In the orthorhombic model (*Fdd*2), ω_1, T_1 sites split into two sets of nonequivalent T positions, i.e., T_1 and T'_1 (each one of multiplicity 8), Ga atoms only occupy T'_1 sites. Concerning the structures with a tetragonal lattice, we have considered three different Ga distributions, i.e., τ_1, τ_2, and τ_3. In the first, the symmetry equivalence between the two T_2 sites in the primitive cell is broken, and Ga atoms occupy the four T_1 sites at the neighbors of one of the T_2 sites. Accordingly, in this model there is a 20% of violations of Loewenstein's rule. In the case of τ_2 and τ_3 models, Ga atoms occupy one site T_1 and one site T_2 per NAT building unit, respectively. As a result, only one symmetry element of the original $I\bar{4}2d$ is kept, namely, a C_2 axis parallel to the x and z directions, respectively.

(15) Wu, F. Y. *Rev. Mod. Phys.* **1982**, *54*, 235.
(16) Sanz, J.; Herrero, C. P.; Robert, J.-L. *J. Phys. Chem. B* **2003**, *107*, 8337.
(17) Saunders, V. R.; Dovesi, R.; Roetti, C.; Causà, M.; Harrison, N. M.; Orlando, R.; Zicovich-Wilson, C. M. *CRYSTAL98 User's Manual*; Università di Torino: Turin, 1999.
(18) Becke, A. D. *J. Chem. Phys.* **1993**, *98*, 5648.
(19) Lee, C.; Yang, W.; Parr, R. G. *Phys. Rev. B* **1988**, *37*, 785.
(20) The CRYSTAL Web Page, URL http://www.CRYSTAL.UNITO.IT.
(21) Doll, K.; Saunders, V. R.; Harrison, N. M. *Int. J. Quantum Chem.* **2001**, *82*, 1.
(22) Civalleri, B.; D'Arco, P.; Orlando, R.; Saunders, V. R.; Dovesi, R. *Chem. Phys. Lett.* **2001**, *348*, 131.

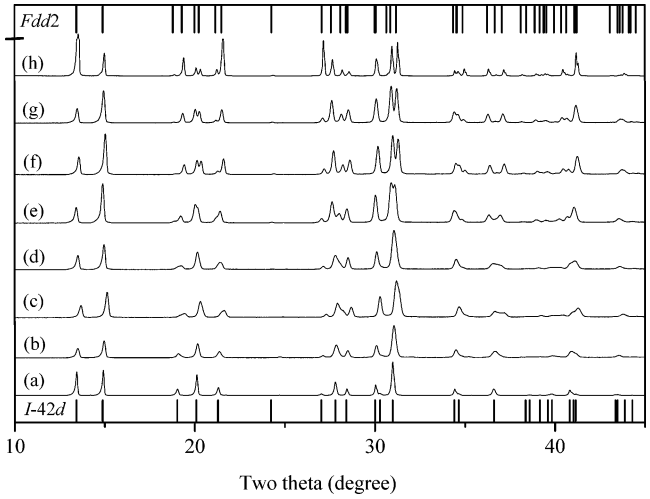

Figure 1. Powder XRD patterns of the products obtained from a series of syntheses performed under different conditions: (a) NAT-100-3, (b) NAT-150-3, (c) NAT-150-5, (d) NAT-150-7, (e) NAT-150-10, (f) NAT-150-14, (g) NAT-150-23, and (h) NAT-200-14 samples. The intensity axis is broken near its top in order to cut the intensity of the first, very intense X-ray peak of the upper trace.

3. Results and Discussion

Figure 1 shows the powder XRD patterns of the products obtained from a series of syntheses performed at 150 °C for different periods (3−23 days) of crystallization. Included as bottom and top traces for comparison are the patterns of NAT-100-3 and NAT-200-14 which are good examples for the disordered and ordered gallosilicate NAT materials, respectively (see below and Table 2). It can be clearly seen that the initial crystallization of a tetragonal phase is followed by its transformation to an orthorhombic phase. Comparison of the patterns in Figure 1 with those in our recent work[10] reveals that the materials obtained after 3 and 23 days of heating would correspond to those previously denoted as TNU-3 (indexed as tetragonal $I\bar{4}2d$) and TNU-4 (orthorhombic *Fdd*2), respectively. The XRD pattern of NAT-150-14 was also found to be essentially the same as that of TNU-4. For intermediate crystallization products, in contrast, there is a broadening of certain reflections followed by their splitting as the crystallization time increases. This can be more clearly seen in Figure 2 where the selected region of the XRD patterns in the range $2\theta = 26-30°$ is shown. This region comprises the (400), (321), and (112) reflections in space group $I\bar{4}2d$, and (440), (151), (511), and (022) or (202) reflections in space group *Fdd*2. Note that an X-ray peak occurring around $2\theta = 28.2°$, which corresponds to the (511) reflection of the orthorhombic materials, is not allowed for the tetragonal ones. As marked with arrows in Figure 2, however, this reflection is clearly visible in the XRD patterns of intermediate crystallization products and becomes stronger with increasing the crystallization time up to 14 days. The same trend can be observed for the peak around $2\theta = 36.4°$, assigned to the (171) reflection of NAT-150-23 (Figure 1). Furthermore, several peaks in the XRD patterns of the materials obtained from 5, 7, and 10 days of heating are broader than the corresponding peaks of the tetragonal NAT-150-3, which cannot be caused by the presence of a material similar to NAT-150-23 as an impurity phase in NAT-150-3. These observations suggest that the materials obtained after 5, 7, and 10 days of heating at 150 °C are not physical mixtures of the end members, but they show an orthorhombic distortion the degree of which increases with increasing the crystallization time.

Table 2 lists the crystallographic data for the NAT-type gallosilicate molecular sieves prepared here. These data reveal that the powder XRD patterns of all the materials can be successfully indexed in the tetragonal space group $I\bar{4}2d$ and/or in the orthorhombic space group *Fdd*2. This again suggests that the intermediate crystallization products are not physical mixtures of the tetragonal and orthorhombic phases. The most interesting result is that, for a given crystallization temperature (150 °C), the unit cell parameter *b* in the orthorhombic indexing is larger at a longer period of crystallization, while the opposite is observed for the unit cell parameter *a*. Here, we have taken the dimensionless parameter, δ_o, which is defined by $(b - a)/(b \times a)^{0.5}$, using the unit cell parameters *b* and *a* obtained from the orthorhombic indexing, as a quantitative measure of the degree of orthorhombic distortion from the idealized tetragonal symmetry of the gallosilicate NAT materials. A plot of the orthorhombic distortion versus the time of crystallization at 150 °C is given in Figure 3. Notice that the degree of orthorhombic distortion increases continuously with increasing the crystallization time from 3 to 14 days and then levels off for longer periods. Figure 3 also shows that the distortion curve may pass through the zero point (ideal tetragonal symmetry) only for a very short time of crystallization at 150 °C. This implies that even for NAT-150-3, the true symmetry may be orthorhombic. As seen in Table 2, on the other hand, NAT-100-3-s shows the smallest δ_o value (0.004) among the materials prepared here. The XRD pattern of this material, which is given as the bottom trace in Figure 1, is satisfactorily indexable as tetragonal and shows quite narrow peaks compared to those from other materials, suggesting that it may actually be a perfect or almost perfect tetragonal phase. It can also be noted from Table 2 that for a given crystallization time the orthorhombic distortion is smaller at a lower crystallization temperature, which is consistent with the trend reported in our previous work.[12] Apparently, the observed increase in the degree of orthorhombic distortion with increasing the crystallization time up to 14 days cannot be rationalized by differences in the framework composition, despite the fact that there is a noticeable but small change in the bulk Si/Ga ratios from ca. 1.7 for the less distorted materials to ca. 1.6 for the most distorted ones. In fact, the data in Table 2 reveal that the bulk Si/Ga ratios of all the NAT materials with $\delta_o \geq 0.010$ are essentially identical to one another, within experimental error (1.58 ± 0.03), while the range of their orthorhombic distortion is rather large (0.012−0.027). Moreover, the distortion is not simply related to a change in the distribution of countercations, since the difference between ordered and disordered materials persists after K^+ ion exchange (Table 2).

Table 2 also shows that as the orthorhombic distortion increases the water content of the zeolites decreases from approximately 21 to 16 molecules per orthorhombic unit cell. This variation of the water content is not accompanied by a similar trend in unit cell volume, which for the orthorhombic description is constant within 1% for all the materials prepared here. However, the decrease in water content as the orthorhombic distortion increases is accompanied by an increase in the temperature (T_{max}) for the desorption of water. It is interesting

Table 2. Crystallographic and Physical Data for the NAT-Type Gallosilicate Materials

sample ID	crystallization conditions[a] (*T*/*t*, °C/days)	unit cell parameters and volume: space group $I\bar{4}2d$ *a*, Å	*c*, Å	*V*, Å^3	space group *Fdd*2 *a*, Å	*b*, Å	*c*, Å	*V*, Å^3	$\delta_o \times 10^{2}$ [b]	Si/Ga ratio[c]	H_2O/uc[d]	T_{max},[e] °C
NAT-100-2	100/2	13.155	6.654	1151.5	18.564	18.670	6.656	2306.9	0.569	1.70	19.4	295
NAT-100-3	100/3	13.147	6.643	1148.2	18.550	18.650	6.643	2298.2	0.538	1.68	19.7	292
NAT-100-3-s	100/3[f]	13.197	6.663	1160.4	18.632	18.702	6.664	2322.1	0.375	1.72	20.9	292
NAT-100-7	100/7	13.185	6.661	1158.0	18.591	18.713	6.662	2317.7	0.654	1.62	19.1	305
NAT-150-3	150/3	13.168	6.666	1155.9	18.554	18.676	6.660	2307.8	0.655	1.55	17.6	312
NAT-150-5	150/5	13.164	6.663	1154.6	18.492	18.714	6.659	2304.4	1.193	1.58	17.3	315
NAT-150-7	150/7	13.163	6.665	1154.8	18.468	18.743	6.658	2304.6	1.478	1.59	17.2	318
NAT-150-10	150/10				18.433	18.785	6.659	2305.7	1.892	1.55	17.0	332
NAT-150-14	150/14				18.383	18.848	6.656	2306.2	2.498	1.57	16.4	332
NAT-150-23	150/23				18.374	18.862	6.658	2307.5	2.621	1.57	16.3	334
NAT-200-14	200/14				18.372	18.872	6.657	2308.1	2.685	1.60	16.3	319
NAT-200-14-s	200/14[f]				18.380	18.873	6.660	2310.3	2.647	1.58	16.3	338
NAT-200-28	200/28				18.377	18.878	6.658	2309.8	2.690	1.59	16.4	330
K-NAT-150-3[g]		13.769	6.541	1240.1	19.277	19.624	6.524	2468.0	1.784			
K-NAT-150-23[g]					19.090	19.824	6.522	2468.2	3.773			

[a] Performed under slow rotation (60 rpm), unless otherwise stated. [b] Degree of orthorhombic distortion defined as $(b - a)/(b \times a)^{0.5}$. [c] Determined by elemental analysis. [d] Determined from TGA assuming an orthorhombic unit cell with 40 T-atoms. [e] Temperature of the endothermic peak maximum in the DTA. [f] Performed under static conditions. [g] K^+-exchanged materials.

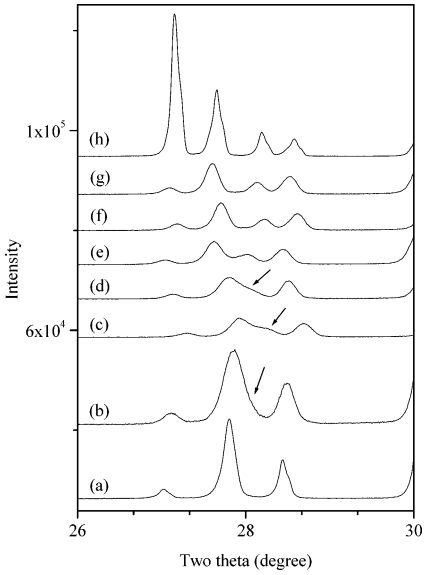

Figure 2. A selected zone of the same powder XRD patterns shown in Figure 1. The arrows point to the (511) reflection of the orthorhombic NAT materials, showing that the apparent broadening of some reflections at the initial stages of the transformation is due to a change in the crystal symmetry.

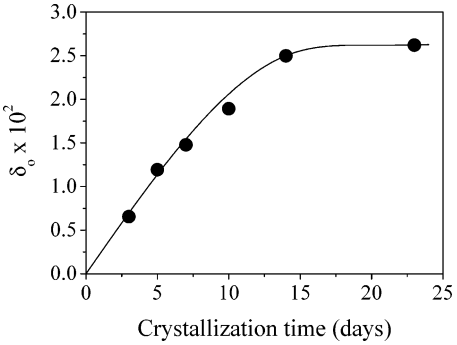

Figure 3. Orthorhombic distortion (δ_o) in gallosilicate NAT materials vs time of crystallization at 150 °C. δ_o is defined as $(b - a)/(b \times a)^{0.5}$, using the unit cell parameters *b* and *a* obtained from the orthorhombic indexing (see Table 2).

to note that, according to the literature,[23,24] aluminosilicate NAT materials with tetragonal symmetry and a disordered distribution of Si and Al atoms are named tetranatrolite and usually contain $16H_2O$/40T. However, the same type of natural materials may contain a larger amount of water, up to $24H_2O$/40T, and they are called paranatrolite.[24] While paranatrolite is reported to easily lose water in air to give tetranatrolite,[25] this does not happen in our gallosilicate synthetic materials, in which the water content apparently depends on the Si, Ga ordering and/or symmetry.

Further evidence for a continuous and smooth change in the structure of the NAT-type gallosilicate materials obtained at a given temperature (150 °C) for different periods (3−23 days) of crystallization is given by ^{29}Si MAS NMR spectroscopy. As seen in Figure 4, this series of materials displays a gradual change in the relative intensities of all the ^{29}Si resonances that ends up for long periods of crystallization in a spectrum dominated by only two very prominent resonances around −84 and −94 ppm. Recall that these six materials prepared here have essentially the same bulk Si/Ga ratio. Therefore, it is clear from Figure 4 that there is a continuous increase in the Si, Ga ordering, as the crystallization time increases. As already discussed in our previous work,[10] on the other hand, the two prominent ^{29}Si NMR resonances appearing around −84 and −94 ppm correspond to Si(3Ga) and Si(2Ga) environments, respectively. However, their integral intensity ratio was found to be always slightly larger than 2:1 which is the expected value for a random but Loewensteinian distribution of Si and Ga in a NAT material with Si/Ga = 1.50. For example, deconvolution of the ^{29}Si MAS NMR spectrum of NAT-150-23 reveals an intensity ratio of 2.3:1 for its two prominent resonances, suggesting a highly but incompletely ordered distribution of Si and Ga over the tetrahedral sites of the framework. The increased ordering in the distribution of Si and Ga with increasing the crystallization time is further supported by the ^{71}Ga and ^{23}Na MAS NMR spectra given in Figures 5 and 6, respectively. For both quadrupolar nuclei with $I = {}^3/_2$, the gradual development of a line shape of the central transition dominated by second-order quadrupolar interactions is indicative of an increased degree of local order.

(23) Mikheeva, M. G.; Pushcharovskii, D. Y.; Khomyakov, A. P.; Yamnova, N. A. *Sov. Phys. Crystallogr. (Engl. Transl.)* **1986**, *31*, 254.
(24) Pechar, F. *Z. Kristallogr.* **1989**, *189*, 191.
(25) Chao, G. Y. *Can. Mineral.* **1980**, *18*, 77.

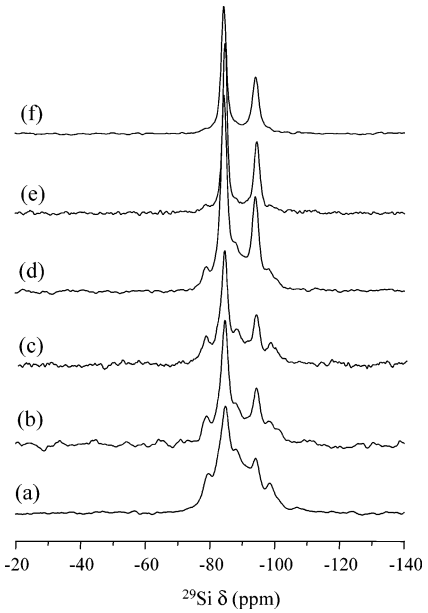

Figure 4. ^{29}Si MAS NMR spectra of a series of gallosilicate NAT materials obtained after heating at 150 °C for different periods of crystallization: (a) NAT-150-3, (b) NAT-150-5, (c) NAT-150-7, (d) NAT-150-10, (e) NAT-150-14, and (f) NAT-150-23.

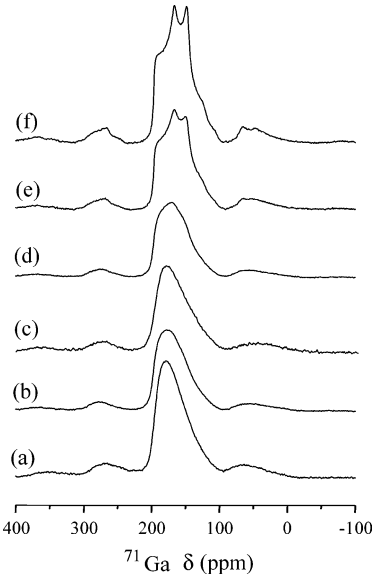

Figure 5. ^{71}Ga MAS NMR spectra of (a) NAT-150-3, (b) NAT-150-5, (c) NAT-150-7, (d) NAT-150-10, (e) NAT-150-14, and (f) NAT-150-23.

The characterization results presented so far have shown beyond doubt that the observed transformation does not involve a phase segregation, a change in topology, or any significant change in chemical composition but rather a smooth structural change related to the ordering of Si and Ga in the NAT framework. A next logical step would be to ascertain whether such a transformation really needs to occur at the crystallization medium under synthesis conditions, i.e., in situ rather than being able to occur simply by heating. To answer this question, we heated the NAT-150-3 and NAT-150-23 materials at 200 °C for 7 days in the absence or in the presence of water (1 g solid per 20 mL water) and then recorded their powder XRD patterns. When compared to the patterns of the corresponding parent materials, no noticeable changes in the position and relative intensity of X-ray peaks were detected. The same conclusion

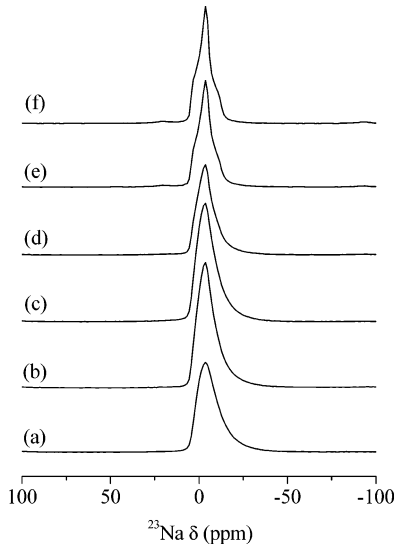

Figure 6. ^{23}Na MAS NMR spectra of (a) NAT-150-3, (b) NAT-150-5, (c) NAT-150-7, (d) NAT-150-10, (e) NAT-150-14, and (f) NAT-150-23.

was also drawn from comparison of the ^{71}Ga and ^{23}Na MAS NMR spectra of NAT-150-3 and NAT-150-23 recorded at 150 °C (Supporting Information Figure 1S) with the spectra of the corresponding materials taken at room temperature (Figures 5 and 6). These results clearly show that the disordered gallosilicate NAT material transforms in situ to its ordered version, which is a strong suggestion of a solution-mediated mechanism for the transformation. On the other hand, the yield of solids between 3 and 23 days of crystallization time at 150 °C was found to remain nearly constant (10.1 ± 0.2 wt %). Only at 100 °C and a very short crystallization time (1 day), a much smaller yield (<0.5 wt %) was obtained. Thus, the transformation does not require the precipitation of fresh solid, suggesting that the disordered gallosilicate NAT phase is metastable and transforms into the ordered phase by Ostwald's ripening through a dissolution/recrystallization process. However, the ripening in our case cannot be simply considered as a matter of dissolution of the less stable phase and separate crystallization of the more stable phase, since the intermediate crystallization products are not physical mixtures but materials with an intermediate degree of ordering (see above). To gain a better understanding of this intriguing phenomenon, therefore, we focused our attention to the NAT-100-3-s and NAT-200-28 materials that can be regarded as the most disordered and ordered phases among the gallosilicates prepared here, respectively, in view of their XRD patterns and calculated δ_o distortion values. The ^{29}Si MAS NMR spectra of NAT-100-3-s and NAT-200-28 together with the simulated spectra and their deconvoluted components are shown in Figure 7, and results from the spectral deconvolution are summarized in Table 3. It should be noted here that the best-simulated spectra were obtained when the experimental ones for NAT-100-3-s and NAT-200-28 are deconvoluted into 9 and 7 components, respectively.

For a Si/Ga ratio of 1.50, complete ordering of Si and Ga atoms in the NAT topology requires the splitting of the high multiplicity site T_1 into a Si site (T_1) and a Ga site (T'_1) plus full occupancy of the low multiplicity site T_2 by Si atoms, leading to the orthorhombic structure. This configuration (and its symmetrical one, related by a mirror plane) is the only ordered one obeying Loewenstein's rule if Si/Ga = 1.50.

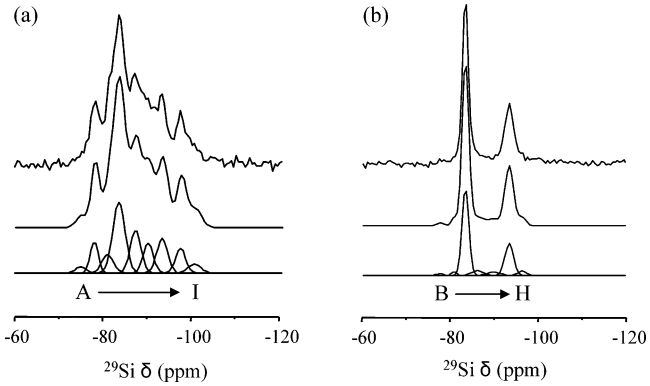

Figure 7. ^{29}Si MAS NMR spectra of (a) NAT-100-3-s and (b) NAT-200-28 materials which are the most disordered and the most ordered phases, respectively, among the NAT gallosilicates prepared in this study: experimental (top); simulated (middle); deconvoluted components (bottom). The deconvoluted ^{29}Si NMR components for these two materials are denoted (from left to right) as lines A−I and lines B−H, respectively.

Although no structural data on the Na form of the fully disordered and ordered NAT materials with a Si/Ga ratio of exactly 1.50 have been reported yet, the detailed crystal structures on the corresponding cation form of two materials with Si/Ga ratios $\approx$ 1.5, in which the distribution patterns of Ga atoms are almost disordered and ordered, respectively, are available in the literature.[26,27] Also, there is a linear relationship between the ^{29}Si chemical shift of a given Si(*n*Ga) species and the average Si−O−T angle in microporous gallosilicate materials,[10,28,29] in analogy to Si(*n*Al) species in aluminosilicate zeolites. Using the equation of Cho et al.[10] and the reported average T−O−T angles for the crystallographically different T-sites in these two gallosilicate NAT materials, therefore, the ^{29}Si MAS NMR chemical shifts of Si(*n*Ga) species with n = 0−4 over each Si site in NAT-100-3-s and NAT-200-28 were calculated and are listed in Table 3. Despite both the empirical nature of the relationship used in calculating the chemical shifts and the possible inaccuracy of the average T−O−T angles employed, a close match between the predicted ^{29}Si chemical shifts and the experimental values is observed for both materials, suggesting that the assignments of their ^{29}Si NMR resonances to the specific structural units listed in Table 3 may be reliable. However, it should be noted that the Si/Ga ratios of NAT materials calculated from their ^{29}Si MAS NMR spectra following the assignments in Table 3 differ considerably according to the type of the T-atom distribution considered. In the case of NAT-100-3-s whose XRD pattern is indexable both as tetragonal and orthorhombic, in fact, Si/Ga ratios of 1.73 and 1.49 were derived from the tetragonal and orthorhombic assignments of its ^{29}Si MAS NMR spectrum, respectively. The value (1.72) determined by elemental analysis agrees well with the Si/Ga_{nmr} ratio calculated from the tetragonal assignment. To further establish the reliability of the strategy used for the assignments of the ^{29}Si MAS NMR spectra in Figure 7, we calculated the ^{29}Si chemical shifts of the fully ordered orthorhombic aluminosilicate NAT material (space group *Fdd*2) with Si/Al = 1.5 using the published crystallographic data[30,31] of two materials with the same space group and Si/Al ratio and the equations of Ramdas and Klinowski[32] and Radeglia and Engelhardt.[33] As seen in Supporting Information Table 2S, the two intense ^{29}Si NMR resonances around −88 and −95 ppm with an intensity ratio of 2:1, which have been repeatedly reported for this material,[34,35] can be more specifically assigned to Si_1(3Al) and Si_2(2Al) species, respectively. This is in agreement with the reported structure, in which all the Si atoms in the fully ordered aluminosilicate NAT are always situated in sites T_1 and T_2 that are surrounded by three and two Al atoms, respectively.[30]

As described above, the preeminence of Si_1(3Ga) and Si_2(2Ga) resonances in the ^{29}Si MAS NMR spectrum of NAT-200-28 is a clear indication of a very high degree of order. However, the deconvolution results in Figure 7 and Table 3 suggest that NAT-200-28 is not perfectly ordered, because the relative intensity of the Si_1(3Ga) and Si_2(2Ga) resonances is 2.6:1 instead of 2:1. Furthermore, additional intensity is present as poorly resolved, low intensity shoulders on either side of the two main resonances. This could be due to the incomplete transformation, the Si/Ga ratio slightly exceeding the required value (1.50) for a complete ordering, or to both. The orthorhombic distortion curve in Figure 3 shows that at 150 °C the transformation apparently stops around $\delta_o = 0.027$. Also, the data in Table 2 suggest that there is actually an upper limit for the orthorhombic distortion at $\delta_o = 0.0268 \pm 0.0002$, when the synthesis was performed at 150 °C for 3−23 days. In fact, deconvolution of the ^{29}Si MAS NMR spectra in Figure 4 indicates that none of the materials showing this degree of distortion are completely ordered, since the ratio of Si_1(3Ga) and Si_2(2Ga) resonances is always somewhat higher than 2:1 and small additional lines are still present. As seen in Table 2, on the other hand, the six gallosilicate NAT materials prepared at the same temperature (150 °C) for different periods (3−23 days) of crystallization time show bulk Si/Ga ratios slightly over 1.50 (1.58 ± 0.03). Interestingly, all the Si/Ga ratios (i.e., $Si/Ga_{nmr,Fdd2}$ ratios) of these materials derived from the ^{29}Si MAS NMR data using the orthorhombic assignment were found to be quite similar to one another (1.50 ± 0.03; see Supporting Information Table 3S). These values are slightly smaller than the values determined by elemental analysis and very close to the Si/Ga ratio (1.50) required for a complete ordering. Although this result looks noticeable, the calculation by ^{29}Si MAS NMR of Si/Ga ratios in these intermediate materials is seriously limited by the different assignments for the deconvoluted ^{29}Si components for the ordered and disordered distributions.

To gain some more insight into the microscopic processes involved in the disorder−order transformation, periodic ab initio calculations performed on some selected models with NAT topology have been considered. Independently of the mechanism through which the recrystallization proceeds, the whole effective transformation energy can be decomposed as a sum of terms corresponding to simple Si−Ga exchange reactions. Each of these exchange reactions may be energetically favored or not,

(26) Malinovskii, Y. A.; Dadashov, M. S.; Bondareva, O. S.; Minachev, K. M. *Sov. Phys. Crystallogr. (Engl. Transl.)* **1991**, *36*, 316.
(27) Xie, D.; Newsam, J. M.; Yang, J.; Yelon, W. B. *Microstructure and Properties of Catalysts, MRS Symposium Series Proceedings*; Materials Research Society: Pittsburgh, PA, 1988; Vol. 111, pp 147−154.
(28) Newsam, J. M.; Vaughan, D. E. W. *Stud. Surf. Sci. Catal.* **1986**, *28*, 457.
(29) Engelhardt, G.; Michel, D. *High-Resolution Solid-State NMR of Silicates and Zeolites*; John Wiley & Sons: New York, 1987.
(30) Artioli, G.; Smith, J. V.; Kvick, A. *Acta Crystallogr.* **1984**, *C40*, 1658.
(31) Meneghinello, E.; Martucci, A.; Alberti, A.; Di Renzo, F. *Microporous Mesoporous Mater.* **1999**, *30*, 89.
(32) Ramdas, S.; Klinowski, J. *Nature* **1984**, *308*, 521.
(33) Radeglia, R.; Engelhardt, G. *Chem. Phys. Lett.* **1985**, *114*, 28.
(34) Lippmaa, E.; Magi, M.; Samoson, A.; Tarmak, M.; Engelhardt, G. *J. Am. Chem. Soc.* **1981**, *103*, 4992.
(35) Neuhoff, P. S.; Kroeker, S.; Du, L.-S.; Fridriksson, T.; Stebbins, J. F. *Am. Mineral.* **2002**, *87*, 1307.

Table 3. Experimental and Predicted ^{29}Si NMR Chemical Shifts of NAT-100-3-s and NAT-200-28 Materials

NAT-100-3-s (tetragonal, space group $I\bar{4}2d$)								NAT-200-28 (orthorhombic, space group $Fdd2$)							
Si site	multiplicity	average ∠T–O–T[a]	structural unit	^{29}Si δ, ppm from TMS: δ_{pre}[b]	δ_{obsd}[c]		$\Delta\delta$[d]	Si site	multiplicity	average ∠T–O–T[e]	structural unit	^{29}Si δ, ppm from TMS: δ_{pre}[f]	δ_{obsd}[c]		$\Delta\delta$[d]
Si_2	4	139.8	Si_2(4Ga)	−75.0	−74.9 (A)	[2.3]	0.1	Si_2	8	140.3	Si_2(4Ga)	−78.8	−81.1 (C)	[2.8]	−2.3
			Si_2(3Ga)	−81.7	−81.0 (C)	[6.8]	0.7				Si_2(3Ga)	−85.5	−86.4 (E)	[3.6]	−0.9
			Si_2(2Ga)	−88.4	−87.2 (E)	[15.9]	1.2				Si_2(2Ga)	−92.2	−93.6 (G)	[23.7]	−1.4
			Si_2(1Ga)	−95.1	−93.1 (G)	[13.0]	2.0				Si_2(1Ga)	−98.9			
			Si_2(0Ga)	−101.8	−100.3 (I)	[3.4]	1.5				Si_2(0Ga)	−105.6			
Si_1	16	131.6	Si_1(4Ga)	−78.6	−78.0 (B)	[11.3]	0.6	Si_1	16	133.6	Si_1(4Ga)	−75.4	−78.0 (B)	[1.2]	−2.6
			Si_1(3Ga)	−85.3	−83.5 (D)	[26.7]	1.8				Si_1(3Ga)	−82.1	−83.7 (D)	[62.8]	−1.6
			Si_1(2Ga)	−92.0	−90.0 (F)	[11.3]	2.0				Si_1(2Ga)	−88.8	−90.1 (F)	[2.7]	−1.3
			Si_1(1Ga)	−98.7	−97.2 (H)	[9.3]	1.5				Si_1(1Ga)	−95.5	−96.5 (H)	[3.2]	−1.0
			Si_1(0Ga)	−105.4							Si_1(0Ga)	−102.2			
$Si/Ga_{nmr,I\bar{4}2d}$[f] = 1.73 (1.72), $Si/Ga_{nmr,Fdd2}$[f] = 1.49								$Si/Ga_{nmr,Fdd2}$[f] = 1.47 (1.59)							

[a] Average T−O−T angles in degrees from the crystallographic data for a tetragonal, partially disordered gallosilicate NAT material with Si/Ga = 1.50 reported by Malinovskii et al..[26] [b] Predicted chemical shifts from the average T−O−T angles using the equation of Cho et al..[10] [c] Observed chemical shifts (from the deconvolution of the experimental spectra) with their relative intensities given in square brackets. The letters given in parentheses are identification labels as those in Figure 7. [d] $\Delta\delta = \delta_{obs} - \delta_{pre}$, difference between observed and predicted chemical shifts. [e] Average T−O−T angles of the two distinct T-sites essentially occupied by Si in the orthorhombic, almost ordered gallosilicate NAT material with Si/Ga = 1.57 reported by Xie et al..[27] [f] The Si/Ga ratio calculated from the NMR data based on the space group $I\bar{4}2d$ or $Fdd2$ (see text). For NAT-100-3-s, whose powder XRD pattern can be indexed in both groups, both values are given. The values in parentheses are the Si/Ga ratios determined by elemental analysis.

chiefly depending on the nature of the sites occupied by the cations to be exchanged. In the first approximation the energetics of the exchange process will be mainly determined by two facts: (1) the topological nature of the sites involved, in the present case this is just limited to two types, i.e., T_1 and T_2; and (2) the nature of the first neighboring cations of each site, i.e., the violation or not of the extended Loewenstein's rule during the exchange reaction. Each of these cases has been studied separately computing the corresponding exchange energies by means of the total ab initio energies of the four fully relaxed periodic models documented in Table 1.

Concerning case 1, the energy cost of the exchange of a Si−Ga pair initially occupying sites T_1 and T_2, respectively, is estimated as the half difference between the total energies of models τ_2 and τ_3. It arises that the Si−Ga exchange energy between sites is about −7.5 kJ mol^{-1}; i.e., the most stable situation is the one where the lowest number of Si atoms occupy T_1 positions. This result is not surprising if we consider the different strains imposed by the framework topology on the TO_4 units at each site and the different flexibility provided by Si and Ga as T-cations. As shown in our previous work,[36] the stability of secondary building units involving 4-rings is significantly increased when some of their Si atoms are substituted by other cations with a larger volume and a larger electropositivity. This behavior has been attributed to the fact that the 4-ring imposes some degree of deformation of the TO_4 units because of the low number of degrees of freedom allowed by the closure of the ring. Therefore, the less covalent the T−O bonds are, the more flexible is the TO_4 unit and the less energetically demanding is its deformation, giving rise to a more stable structure. In the case of the NAT topology, the strain on T_1 will be, in principle, larger than that on T_2 because three O−T−O bonds of the former are constrained within 4-rings, while in the latter only two O−T−O bonds are in such a situation. Accordingly, the stabilization provided by the substitution of Si by a more electropositive atom like Ga will be larger in T_1 than in T_2, in agreement with the calculated relative stabilities.

(36) Blasco, T.; Corma, A.; Díaz-Cabañas, M. J.; Rey, F.; Vidal-Moya, J. A.; Zicovich-Wilson, C. M. *J. Phys. Chem. B* **2002**, *106*, 2634.

Table 4. Averaged Percentages of Si Atoms with *n* Neighboring Ga, i.e., Si(*n*Ga): Total Values and Contributions from Si at T_1 and T_2 for the Simulated Disordered Structures with Different Si/Ga Ratios

n	Si/Ga	0	1	2	3	4
total	1.50	4.09	12.04	23.99	34.62	25.26
	1.53	4.44	12.69	25.01	34.59	23.26
	1.55	4.59	13.15	25.74	34.52	22.00
	1.58	4.83	13.70	26.93	34.56	19.97
T_1	1.50	0.56	10.22	15.45	29.67	19.16
	1.53	0.68	10.62	16.30	29.73	17.44
	1.55	0.75	10.90	16.84	29.72	16.40
	1.58	0.90	11.21	17.53	29.89	14.76
T_2	1.50	3.54	1.82	8.54	4.95	6.10
	1.53	3.76	2.07	8.71	4.87	5.82
	1.55	3.83	2.25	8.90	4.80	5.60
	1.58	3.93	2.49	9.41	4.68	5.21

The most interesting consequence of this phenomenon is that, even in the most disordered tetragonal form, the occupancies at T_1 and T_2 will not be equal, a Ga population in T_1 larger than that in T_2 being expected. This is in agreement with the fact that in these materials T−O distances are shorter for T_2 than for T_1, evidencing lower Ga content in T_2.[26] As regards the case where a Si−Ga exchange introduces one violation of Loewenstein's rule (case 2), on the other hand, the energy cost of the process was calculated to be about 31.8 kJ mol^{-1}, estimated as the difference between the total energies of models ω_1 and τ_1 divided by 4. Since the energy cost of the Si−Ga exchange between T_1 and T_2 sites is about a fourth of the cost of an exchange that introduces a single violation, one can reasonably suppose that the preference of Si to occupy site T_2 will also have a significant influence on the final cation distribution for the NAT topology with Si/Ga = 1.50. Under this hypothesis the simple statistical model described in the Experimental Section has been developed in which the T_2 preference of Si occupation and the Loewenstein's rule are the only constraints for the cation distribution. Using the Monte Carlo sampling procedure the statistical properties of the distribution have been obtained. As given in Supporting Information Table 4S, the ratio between T'_1 and T_2 Ga occupancies in the disordered model is 1.76 for Si/Ga = 1.50, increasing up to 2.05 for Si/Ga = 1.58, which is in good

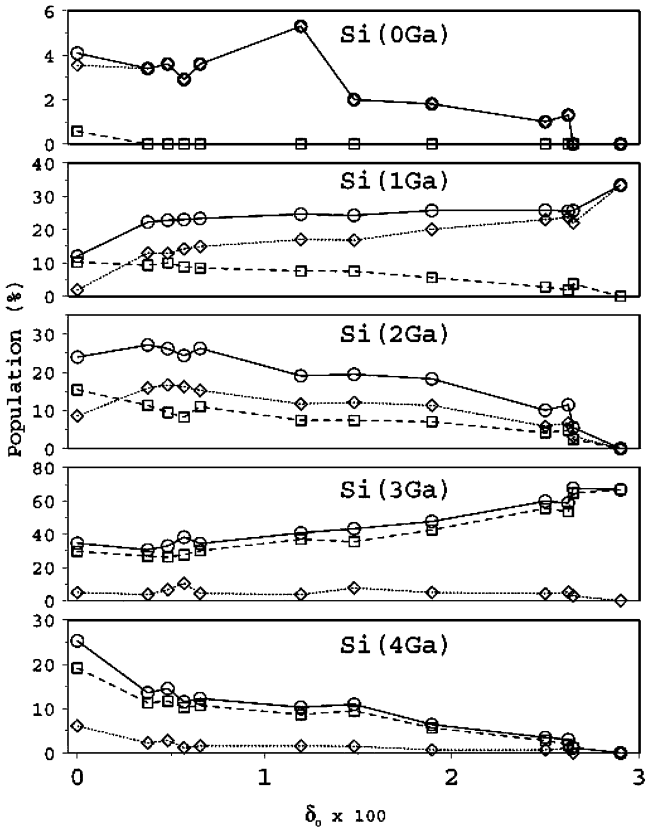

Figure 8. Si(*n*Ga) populations as a function of the orthorhombic distortion. The populations calculated for the "disordered" model derived by Monte Carlo sampling (Si/Ga = 1.50) are shown at $\delta_o = 0.000$, while those corresponding to the ordered model are arbitrarily depicted at $\delta_o = 0.029$. The rest of the values correspond to the experimental ones obtained from the orthorhombic assignment of the ^{29}Si MAS NMR data. The square, diamond, and circle denote T_1, T_2, and total $T(T_1 + T_2)$ populations, respectively.

agreement with the T−O distances featured by the tetragonal gallosilicate NAT material. In contrast, the practically equal occupancy for T_1 and T'_1 indicates that disorder involves mainly the T_1 distribution, giving rise to an averaged tetragonal symmetry.

Table 4 lists the averaged populations of Si atoms in Si(*n*Ga) environments as a function of the Si/Ga ratio of the material and of the T-site, as derived from the simulated disordered structure. Concerning the dependence of the distribution on the material composition, it arises that, being the qualitative trends similar in all cases, there are non-negligible quantitative differences in the distributions when changing the Si/Ga ratio. In particular for Si(2Ga) and Si(4Ga), the environments showing larger absolute variations as the Si/Ga ratio increases, the population exhibits inverse trends. The simulated and experimental Si(*n*Ga) populations are depicted as a function of the orthorhombic distortion in Figure 8. The simulated data (Si/Ga = 1.50) are represented at the limit of minimum distortion (maximum disorder), while at the limit of maximum order (full orthorhombic distortion, arbitrarily set as $\delta_o = 0.029$) the corresponding theoretical values are used. It is particularly interesting that even if the fully tetragonal material ($\delta_o = 0$) could not be synthesized, the simulation data seem to correspond naturally to the experimental trend, even if the error bar caused by the fact that the Si/Ga ratios are greater than 1.50 in the samples is expected to be significant, in particular for Si(2Ga) and Si(4Ga). Actually, as deduced from variations in the relative Si population in Table 4, an increase in the Si/Ga ratio would increase the population of Si(2Ga) while decreasing that of Si(4Ga). This validates both the proposed assignation for the ^{29}Si MAS NMR resonances and our model of disorder constrained simultaneously by Loewenstein's rule and the preference of Si atoms to occupy site T_2.

Since the transformation from the disordered material to the ordered one necessarily requires the breaking and rebuilding of Si−O−Ga and Si−O−Si bonds, together with Ga and Si migrations, and it occurs in the presence of the mother liquor, we believe that it must occur via a dissolution/recrystallization process. Most likely, the driving force for the recrystallization is the preference of Si to occupy the low multiplicity site (constraining Ga to occupy the other site) while still obeying Loewenstein's rule. Therefore, for a Si/Ga ratio close to 1.50, the high multiplicity site is split into two sites occupied by Si (T_1) or Ga (T'_1), respectively. On the other hand, we note that the ordered model offers only two unique configurations (related by a mirror symmetry operator), while the disordered model may be achieved by significantly many more different configurations. This suggests that the latter model may be initially favored for the simple reason that it is much more probable than the former. However, the ordered material is the most stable phase, as the number of Si atoms in site T_1 is minimized and, therefore, the initially formed disordered material evolves, since the very beginning, toward the orthorhombic form. The smooth transformation without phase segregation is possible, because of the fact that disordered and ordered domains may be as small as one single unit cell without significant change in unit cell volume.

Finally, we measured the powder XRD patterns of NAT-100-3-s and NAT-200-28, which are the most disordered and ordered phases, respectively, among the gallosilicate NAT materials prepared here, during in situ heating under vacuum to a residual pressure of 5×10^{-3} Torr at different temperatures. These experiments were performed because a sharp parallelism exists between the orthorhombic distortion and the T_{max} value of the endothermic DTA peak (Table 2). The in situ XRD patterns in Figure 9 show that NAT-100-3-s is already much modified at 320 °C. This is slightly higher than the temperature range at which the endothermic weight loss step occurs.[10] However, increasing temperature to 320 °C causes no detectable changes in the XRD pattern of NAT-200-28. As a result, the temperature (520 °C) at which we cannot recognize any of the unique X-ray reflections (like those around 13.5 and 14.9°) from NAT-200-28 was found to be considerably higher than that (440 °C) from NAT-100-3-s. Since the bulk Si/Ga ratio (1.72) of the former is slightly higher than that (1.59) of the latter, it is clear that the observed difference in their thermal stability should be attributed mainly to the difference in T-atom orderings of these two materials. Figure 9 also reveals that both materials transform to crystalline phases characterized by similar but slightly different XRD patterns, most likely corresponding to the gallosilicate analogues of metanatrolite, i.e., to their dehydrated products, when heated under vacuum. Unfortunately, the calcined materials began losing crystallinity with rehydration at room temperature, thus preventing an analysis of their symmetries. It has long been recognized that the thermal stability, acidity, and catalytic activity of zeolites could differ

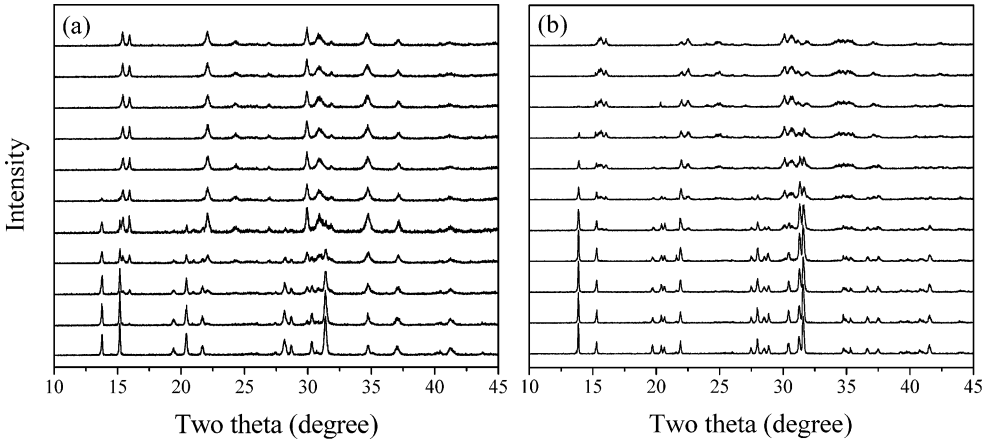

Figure 9. Powder XRD patterns of (a) NAT-100-3-s and (b) NAT-200-28 recorded during in situ heating under vacuum to a residual pressure of 5×10^{-3} Torr at intervals of 40 °C. The bottom and top traces are the patterns measured at 200 and 600 °C, respectively.

according to the manner in which heteroatoms are spatially distributed over the available T-sites.[2] To the best of our knowledge, however, there are few examples where the effects of T-atom distributions in zeolites on their physicochemical and catalytic properties have been clearly established. The present study demonstrates that different distributions of Ga and Si in the NAT framework give rise to at least two well-defined physicochemical differences: the amount of zeolitic water retained and the thermal stability.

4. Conclusions

For gallosilicate natrolite materials, a smooth and slow disorder−order transformation was found to occur in situ under crystallization conditions and without phase segregation. During most of the solution-mediated transformation, there are no significant changes in yield or chemical composition. A series of materials with different degrees of Si−Ga order ranging from a very highly disordered phase to an almost completely ordered one has been prepared and characterized. The driving force for the transformation appears to be a preferential siting of Si to occupy the low multiplicity site and of Ga to occupy half of the high multiplicity site. If Loewenstein's rule is obeyed, for the NAT topology with a Si/Ga ratio of 1.50, the ordered model is unique and such a preferential siting forces the high multiplicity site to split, yielding an ordered distribution that has only two symmetrical configurations. By contrast, the disordered distribution, which is not fully disordered and already showed preferential siting, affords many different configurations, making it kinetically favored. Two significant physicochemical differences between the ordered and disordered materials have been found: the water content decreases and the thermal stability increases when the T-atom ordering increases.

Acknowledgment. Financial support for this work was partially provided by the Korea Science and Engineering Foundation under Grant No. R02-2003-000-10087-0 to S.B.H. We thank Dr. E. Rodrigues (Instituto de Matemáticas, UNAM) for helpful discussion. C.Z.-W. acknowledges support from SEP-FOMES2000 through Project "Cómputo Científico" for unlimited CPU time on the IBM-p690 32-processor supercomputer at UAEM.

Supporting Information Available: Additional information as noted in the text (PDF). This material is available free of charge via the Internet at http://pubs.acs.org.

JA046921H